PAPER • **OPEN ACCESS**

Insights into spatial inhomogeneity in an oxygen plasma from cavity ringdown spectroscopy

To cite this article: Samuel D A Rogers *et al* 2024 *Plasma Sources Sci. Technol.* **33** 015005

OPEN ACCESS
IOP Publishing
Plasma Sources Science and Technology
Plasma Sources Sci. Technol. **33** (2024) 015005 (11pp)
https://doi.org/10.1088/1361-6595/ad1a79

Insights into spatial inhomogeneity in an oxygen plasma from cavity ringdown spectroscopy

Samuel D A Rogers[1], Amelia Bond[2], Robert Peverall, Gus Hancock and Grant A D Ritchie*

Department of Chemistry, Physical and Theoretical Chemistry Laboratory, The University of Oxford, South Parks Road, Oxford OX1 3QZ, United Kingdom

E-mail: grant.ritchie@chem.ox.ac.uk

Received 21 September 2023, revised 7 December 2023
Accepted for publication 3 January 2024
Published 12 January 2024

Abstract

Cavity ringdown spectroscopy has been used to investigate the translational and rotational temperatures of the $v = 0$ and 1 vibrational levels of $O_2(X)$ in an inductively coupled plasma at 100 mTorr (13.332 Pa) pressure. All rotational states probed display a clear increase in temperature as plasma power increases: at fixed power, the translational temperature appears largest for rotational states in $v = 1$ ($J = 7$, 16, 17, 22) and lowest in the low energy states ($J = 1$, 18, 19) in $v = 0$; highly excited rotational states ($J = 28$, 30, 31) of $v = 0$ show intermediate behaviour. The rotational temperature values behave similarly. These observations are consistent with the effects of plasma inhomogeneity and can be interpreted with a simple one-dimensional model whereby the pressure, temperature and mole fractions of the various species across the chamber (and arms) are approximated with rational profiles and the corresponding line-of-sight averaged densities and temperatures calculated. This basic model is reasonably successful at reproducing the observations for $O_2(X, v = 0)$ and $O(^3P)$ densities. The fact that resolving several rotational transitions allows spatial variations within the plasma to be inferred from line-of-sight averaged measurements is an extremely powerful result that could be of great utility in future work.

Keywords: oxygen plasma, cavity ringdown, spatial inhomogeneity

1. Introduction

Oxygen plasmas are a fascinating example of an electronegative plasma. Not only are they fundamentally interesting, they are of significant industrial importance having applications in fields such as plasma enhanced chemical vapour deposition, surface treatment, chamber etching of silicon dioxide layers, and plasma sterilisation [1–9]. As such there continues to be wide interest from both academia and industry in improving both experimental and theoretical understanding of these complex systems [10–13]. The chemistry and physics of these plasmas is heavily influenced not only by the presence of negative ions, but also high densities of ground state atoms, $O(^3P)$, and electronically excited molecules, particularly the low-lying metastable state, $O_2(a^1\Delta_g)$. Such is the importance of these species that accurate knowledge of their absolute densities is vital to testing and refining models of both the gas-phase and the gas-surface chemistry occurring in these systems [13–17].

[1] Present address: Department of Chemistry, Wolfson Atmospheric Chemistry Laboratories, University of York, York YO10 5DD, United Kingdom.
[2] Present address: British Antarctic Survey, High Cross, Madingley Road, Cambridge CB3 0ET, United Kingdom.
* Author to whom any correspondence should be addressed.

With these aims in mind, we have recently reported high resolution diode laser-based cavity ringdown measurements of the most important species in a pure oxygen plasma [17–19]. Ground state atomic oxygen, $O(^3P)$, has been probed using the $O(^1D) \leftarrow O(^3P)$ absorption at 630 nm as a function of plasma pressure and power [18]. Measurements included the observation of wall loss kinetics and of the switchover of the plasma from the capacitive *E*-mode of operation to the hotter and denser *H*-mode indicated by an increase in atom density by an order of magnitude (from a few 10^{13} to a few 10^{14} cm^{-3}) [17]. The measured dissociation fractions (≈10% in the *H*-mode) are consistently high predominantly as a result of the slow wall loss of atoms in the aluminium plasma chamber (as defined by the wall loss coefficient, $\gamma \approx 0.003$). The first metastable state of molecular oxygen, $O_2(a)$, has also been measured by cavity ringdown spectroscopy (CRDS), using the Noxon system at 1.9 μm, and found to make up as much as 5% of the total plasma density [19]; while it also shows a clear increase in density at the *E*/*H* switchover this increase is not as marked as for $O(^3P)$. Time resolved measurements also allowed the wall loss coefficient for $O_2(a)$ to be determined ($\gamma \approx 0.003$). These CRDS results have been supported by observations of the plasma emission, in particular from strong atomic emission lines and from the O_2 *b*–X system. The fitting of molecular spectra to simulations enabled determination of both rotational (350–630 K) and vibrational (905 K) temperatures as well as giving an indication of the relative density of $O_2(b)$ as a function of plasma power at a total pressure of 100 mTorr (13.332 Pa) [17].

This work complements that by Wegner *et al* [20] who investigated the *E*–*H* transition in an inductively coupled radio frequency (RF) discharge in pure oxygen over the pressure range 5–15 Pa. Interestingly, three different operation modes were discernible; with increasing RF power (and electron density), the plasma transitions from the *E*-mode to a hybrid *E*/*H*-mode before entering the *H*-mode. In contrast to the optical cavity-based measurements presented here, these researchers utilised vacuum ultraviolet absorption spectroscopy to determine the line-of-sight integrated densities of both the molecular ground state, $O_2(X)$, and the first singlet metastable state, $O_2(a)$. Notably, analysis of the optical emission from the plasma in the wavelength range 763–774 nm provided the rotational temperature of the excited state O_2 (b, $v = 0$) level, and this is assumed to be equal to the gas temperature. In other studies, two-photon laser induced fluorescence has been utilised to measure atomic oxygen; e.g. Corr *et al* [11] have used this technique to study the discharge kinetics of a pure oxygen inductively coupled plasma (ICP) for a total gas pressure ranging from ca. 5–50 mTorr (0.667–6.667 Pa), reporting an increase in number density from 10^{12} cm^{-3} in the *E*-mode to about 10^{14} cm^{-3} in the *H*-mode. We note that the limited spectral resolution of the method precluded any determination of translational temperatures. Other complementary studies of interest include that by Fuller *et al* [21] who derived absolute number densities of $O(^3P)$ from O-atom emission at 844 nm, combined with Ar emission actinometry and modelling, in a transformer-coupled oxygen plasma at a total gas pressure of 10 mTorr (1.333 Pa).

In our work, all of the experimental results were interpreted using a volume averaged kinetic model based on a restricted number of important reactions [17]. This model, which included 34 kinetic processes, was successful in reproducing experimental atom, anion and metastable molecule densities and from it electron densities and temperatures were inferred. At 300 W the electron density is 4×10^9 cm^{-3} and consistent with the large volume of the plasma chamber. However, despite the success of the volume averaged model at reproducing line-of-sight average experimental number densities of multiple plasma species, several features of the CRDS and emission data clearly indicate that the plasma is not homogeneous. In particular, different species tend to show different apparent translational, T_{trans}, and rotational temperatures, T_{rot}, with those that are longest lived showing lower temperatures than those with shorter lifetimes. For example, the T_{rot} values for $O_2(b)$ inferred from the emission studies (ca. 630 K at 300 W) are significantly higher than the values of T_{trans} for the O atoms measured by CRDS (ca. 450 K at 300 W) and reflects both the differing volumes of the plasma that each technique samples and its inherent spatial inhomogeneity. This observation led to the hypothesis that the plasma possesses significant thermal inhomogeneity, with long lived species having sufficient lifetimes to thermally equilibrate with the cool chamber walls and also to potentially penetrate a significant distance into the cold baffle arms which are attached to the chamber to facilitate CRDS (*vide infra*), thereby exhibiting a reduced apparent line-of-sight average temperature.

In this paper we further test this hypothesis by reporting new CRDS measurements on a selection of rotational levels within the $v = 0$ and $v = 1$ states of the electronic ground state $O_2(X)$ as the plasma power is varied. These measurements, on the principal molecular component in the plasma, show unequivocally the effects of inhomogeneity. As expected, the $v = 0$ state, which fills the majority of the arms, show cold (<350 K) apparent line-of-sight averaged values for T_{trans} unless very highly excited rotational states are probed. $O_2(X, v = 1)$ meanwhile appears translationally hot (≈550 K) across all rotational states as a result of it being produced only in the hot plasma and then lost rapidly (by *V*–*T* energy transfer) if it leaves this region. The work demonstrates that CRDS measurements of $O_2(X)$, although line-of-sight averaged, can contain enough information to probe spatial inhomogeneity within the plasma chamber.

Finally, the measurements are interpreted by a simple one-dimensional model of inhomogeneity whereby the pressure, temperature and mole fractions of the various species across the chamber (and arms) are approximated and the corresponding line-of-sight averaged densities and temperatures calculated. This basic model is reasonably successful at reproducing the observations for $O_2(X, v = 0)$ and $O(^3P)$.

2. Experimental details and data analysis

The CRDS measurements were conducted in a water-cooled cylindrical plasma chamber previously described in detail by Peverall *et al* [18] and Bakowski *et al* [22]. The chamber

measures 21 cm × 35 cm (height × diameter), is predominantly constructed of aluminium, and is fitted with a pair of vacuum mirror mounts separated from the main chamber by narrow diameter (id ∼10 mm) baffle arms to protect the cavity mirrors from the plasma environment. Pure O_2 (99.999% BOC) is delivered into the chamber via the baffle arms at a constant flow of 10 sccm and the chamber pressure is maintained at 100 mTorr for all measurements. Power (0–300 W; 13.56 MHz) is supplied to the chamber via a 1.5 turn, planar, double-spiral antenna (diameter ∼20 cm) which is separated from the plasma by a fused silica window. Two high reflectivity concave mirrors ($R > 99.995\%$, radii of curvature −1 m, Layertec) are housed in the vacuum mirror mounts forming an optical cavity and enabling CRDS to be performed as detailed in Peverall *et al* [18] and Rogers *et al* [19]. In these experiments a continuous-wave external cavity diode laser (Toptica GmbH) operating in the range 747–792 nm is used to excite a resonant mode of the cavity, and when the intensity of radiation in this mode reaches a predefined threshold value, an acousto-optic modulator is triggered and acts as a fast switch to stop the laser beam entering the cavity thus beginning a ringdown event [23]. Ringdown signals were detected using a photomultiplier tube (type 9124b EMI). The characteristic exponential decay time of the radiation intensity reflects the losses in the cavity both from the mirrors and absorption. By stepping the laser over the absorption profile and averaging typically 100 ringdown events at each wavelength, a spectrum can be produced. CRD spectra are produced from measured ringdown times according to:

$$\alpha(\upsilon) = \frac{1}{c}\left(\frac{1}{\tau(\upsilon)} - \frac{1}{\tau_0(\upsilon)}\right), \tag{1}$$

where $\alpha(\upsilon)$ is the frequency dependent absorption coefficient averaged over the line-of-sight, c is the speed of light, $\tau_0(\upsilon)$ is the ringdown time without absorber (taken by fitting a baseline to the CRD spectra) and $\tau(\upsilon)$ is the ringdown time with the absorber present. Under conditions of homogeneity, these spectra, along with Gaussian fits to the data (Doppler broadening dominates at 100 mTorr), would allow direct calculation of T_{trans} as the full width at half maximum (FWHM), $\Delta\upsilon$, of a Doppler broadened line is directly related to temperature T by:

$$\frac{\Delta\upsilon}{\upsilon} = \sqrt{\frac{8k_B T \ln 2}{mc^2}}. \tag{2}$$

However, we note that here such an analysis only yields an apparent temperature, because for a sample of non-uniform temperature and density the FWHM of the absorption line no longer directly gives the gas temperature, but can only approximate it. Nevertheless, we still expect the absorption line widths to be at least representative of the line-of-sight average temperature specific for the quantum state being probed. To test that this is so, a simple simulation with conditions *in extremis* (arms at 300 K, 123 mTorr; chamber at 600 K, 100 mTorr, for $J = 1$, 18 and 30 levels) was performed, yielding an absorption lineshape as a weighted sum of two Gaussians. The subsequent (single) Gaussian fit to this lineshape results in at most a 4% error in the returned temperature when compared to the true, rotational state specific, line-of-sight average, where the goodness of fit parameter R^2 is always > 0.9995. Lineshape fitting allows the determination of integrated absorption coefficients, α_{INT}, from which line-of-sight averaged densities, N_{avg}, are extracted using, $\alpha_{\text{INT}} = \sigma_{\text{INT}} N_{\text{avg}}$ where σ_{INT} is the integrated cross section for the transition.

Measurements of $O_2(X)$ utilised absorption within the b–X system, commonly known as the oxygen A band. The density of $O_2(X)$ is sufficiently high that despite the forbidden nature of this electronic transition, the absorption signals are large enough to enable detection on both the (0, 0) and (1, 1) bands and thus gives some indication of the vibrational excitation present within the plasma. It should be noted however that despite the relative ease of the measurements, any interpretation is made more difficult (particularly for $v = 0$) because, whereas other species are, to a first approximation, absent from the baffle arms, $O_2(X)$ fills the arms. Indeed, because the feedstock gas flows along the arms there is actually a pressure gradient along each arm and thus a high density of $O_2(X, v = 0)$ outside of the plasma zone which contributes significantly to absorption measurements and makes it difficult to establish how much of the absorption originates from $O_2(X)$ within the plasma itself (A measurement of the average pressure in the arms is described in section 3, while the functional form of the pressure variation in the arms is discussed in section 4). On top of this there is also the issue of temperature inhomogeneity; when the plasma is on, the species in the central part of the chamber show a translational temperature of the order of 600 K (as derived from emission studies at 300 W[18]) whilst most of the species in the arms are expected to be approximately ambient (300 K). This is a significant confounding influence when it comes to interpreting line-of-sight averaged CRDS data. Despite this difficulty the ability of this spectrometer to probe several rotational lines (in both the (0,0) and (1,1) vibrational bands) enables some insight to be obtained.

3. Results

3.1. Measurements on O_2 (X, $v = 0$)

CRDS spectra were obtained at 100 mTorr (13.332 Pa) total pressure and a range of plasma powers. In order to probe the expected change in apparent T_{trans} with rotational energy, several rotational lines of the (0,0) vibrational band were probed, specifically: $^{\text{p}}P_{12}(1)$, $^{\text{r}}Q_{11}(18)$, $^{\text{r}}R_{12}(19)$, $^{\text{r}}Q_{11}(28)$, $^{\text{r}}Q_{11}(30)$ and $^{\text{p}}P_{12}(31)$. The transitions are labelled according to the scheme, $^{\Delta N}\Delta J_{F'F''}(J'')$ where N is the total angular momentum quantum number excluding spin and the possible values of the total angular momentum quantum number J are $J = N + 1$ (F_1), $J = N$ (F_2) and $J = N - 1$ (F_3). F_i denotes the spin-rotation manifold while $'$ and $''$ labels denote the upper and lower states involved in the transition, respectively. These lines were selected based on the desire to probe a wide range of rotational energies and when possible were selected so that 2 lines could be probed in a single laser scan; this not only

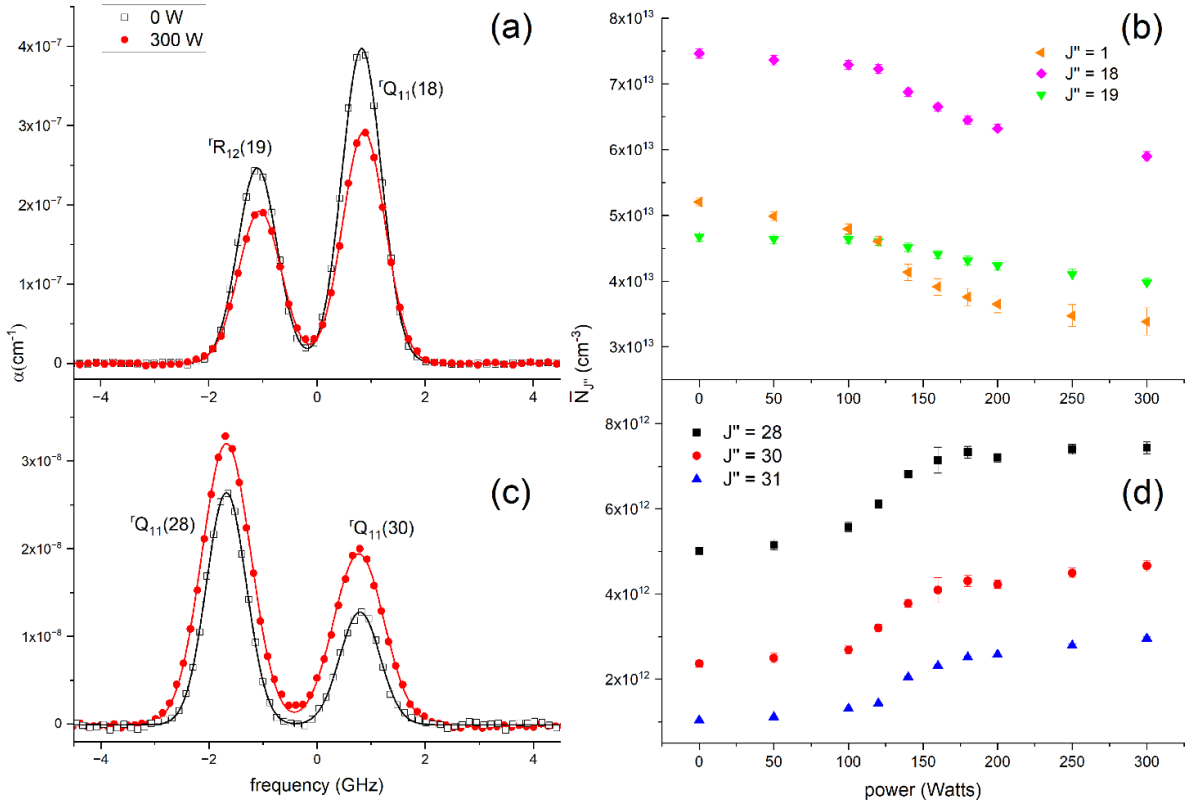

Figure 1. The effect of rotational heating of the gas as power increases. CRD spectra on the oxygen A-band (the (0,0) band) showing (top, (a) and (b)) decreasing line-of-sight averaged absorption as power increases for low J and (bottom (c) and (d)) increasing line-of-sight absorption for high J. The panes (b) and (d) are the line-of-sight averaged rotational state densities derived from CRD spectra (left panes (a) and (c)). Spectra in (a) and (c) are centred around 394 488.351 GHz (13 158.715 cm^{-1}) and 394 683.456 GHz (13 165.223 cm^{-1}), respectively.

provides more data but also enables self-calibration of the frequency scale because the line positions are precisely known from a PGOPHER simulation [24]. This PGOPHER simulation is also able to calculate cross-sections for these magnetic-dipole allowed transitions. For the PGOPHER simulation, the molecular constants and Franck–Condon factors were taken from Yu *et al* [25] and the magnetic dipole moment from Drouin *et al* [26]. Line strengths and positions show very good agreement with the HITRAN database [27].

A small sample of the measured CRD spectra are shown in figure 1. Figure 1(a) shows spectra of $^{r}Q_{11}(18)$ and $^{r}R_{12}(19)$ with and without plasma, while figure 1(c) shows the same for the $^{r}Q_{11}(28)$ and $^{r}Q_{11}(30)$ transitions. As detailed in the previous section, the spectra can be used to find line-of-sight averaged densities and apparent translational temperatures. Unfortunately, because for a thermally inhomogeneous sample the distribution of each rotational state along the beam path will be different, no simple length adjustment can be made to determine the density of O_2(X) in the chamber specifically. The line-of-sight averaged values can never-the-less still be informative, and figure 1(b) shows line-of-sight averaged number densities for each rotational state as a function of plasma power. The lowest J states ($J'' = 1$, 18, 19), shown in figure 1(b) show a decrease in density with increasing power. The reasons for this are three-fold: as power increases the gas in the chamber is heated and hence becomes less dense; as power increases the mole fraction of O_2(X) in the chamber decreases; and as power increases the heating means that the fraction of O_2(X) which is partitioned into the lowest rotational states (particularly $J = 1$) decreases. For the higher J states ($J'' = 28$, 30, 31) (see figure 1(d)) the first two factors once again act to decrease density as power increases, they are however outweighed by the fact that as the gas heats the fraction of O_2(X) partitioned into high J states increases very significantly, e.g. at 300 K around 1 in every 3300 molecules would be in the $J = 31$ state but this increases to 1 in every 210 molecules at 600 K.

Figure 2(a) shows the apparent line-of-sight average translational temperatures, T_{trans}, specific to each of the rotational states as a function of plasma power. At low powers, where the plasma temperature is close to ambient and thus the entire cavity length is of approximately uniform temperature, all the rotational states show the same apparent T_{trans} value, close to 300 K. As power increases however there is once again a significant difference in average temperature between the high J states and the lower J states. In all cases for powers >200 W, the measured T_{trans} increases monotonically with increasing rotational energy. This observation is consistent with the densities in figure 1(b) and can once again be explained by the fact that the population of high J states in the colder baffle

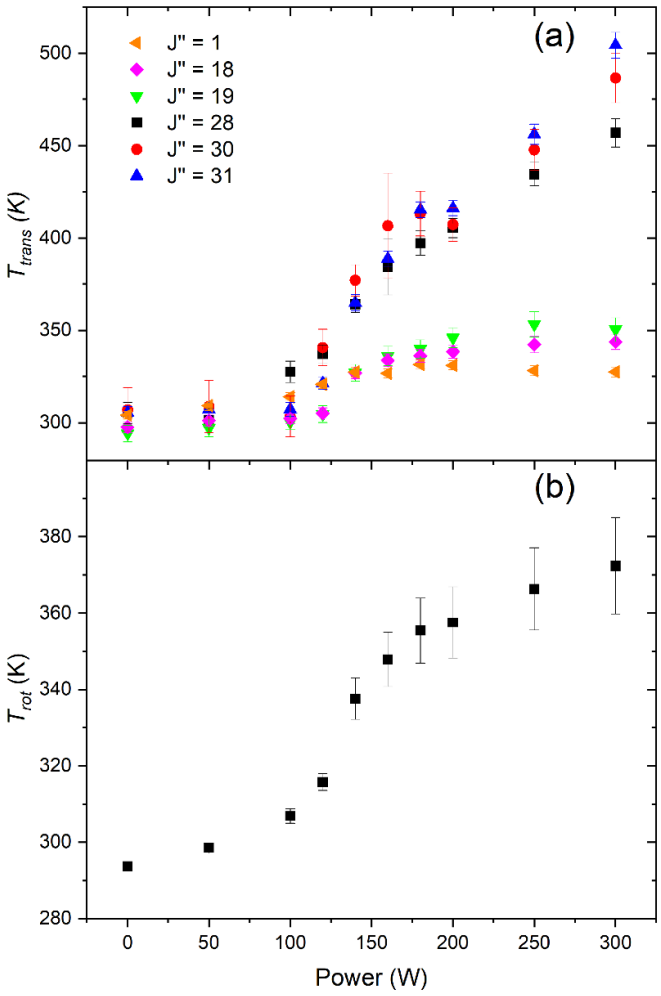

Figure 2. (a) Apparent state specific line-of-sight averaged translational temperatures for the various rotational states of O_2(X). The data show a clear increase in apparent translational temperature with increasing rotational state in the *H*-mode resulting from the different spatial distributions of these states in the thermally inhomogeneous plasma. (b) Rotational temperature derived from the linear fits to Boltzmann plots, whereby the linear fit becomes less appropriate at higher powers, so the temperature becomes less certain.

arms is small and their population in the hotter bulk of the plasma is much higher whilst the opposite is true of the lower *J* states.

When densities of several rotational states are known a Boltzmann plot can be constructed. The data in figure 1 was used to construct a Boltzmann plot at each plasma power. At 0 W the plot was found to be linear ($R^2 > 0.99999$) with a gradient corresponding to a rotational temperature of (293.7 ± 0.6) K (such accuracy is possible because at 0 W the temperature is entirely uniform along the CRDS line-of-sight) and an intercept corresponding to a line-of-sight average density of O_2(X, $v = 0$) of $(3.70 \pm 0.01) \times 10^{15}$ cm^{-3} which is higher than that corresponding to the central chamber pressure (in this instance set to 100 mTorr). This difference is as a result of the flow of gas along the baffle arms which is necessarily associated with a pressure gradient, and thus the pressure in the baffle arms is greater than that in the chamber. By subtracting the expected absorption coefficient from the 35 cm of 100 mTorr oxygen in the chamber itself from the total absorption coefficient, one can determine the line-of-sight average pressure in the arms to be ≈123 mTorr. The precise spatial variation of pressure within the arms can be approximately modelled according to the Poiseuille equation, *vide infra*.

Figure 2(b) shows the rotational temperatures, T_{rot}, derived from the Boltzmann plots, as a function of plasma power. All such plots are influenced by the cool gas in the baffle arms but the temperatures still show a smooth increase with increasing power including a steeper increase at the *E*/*H* switchover. We note that towards higher powers the Boltzmann analysis deviates from linearity (R^2 is reduced to 0.996 at 300 W), and in fact a quadratic fit is much more successful at fitting the data; this non-linearity results in the much larger error bars in figure 2(b) at higher powers when a linear fit is used. This is again the result of thermal inhomogeneity in the plasma with the effect that the Boltzmann plot looks cooler (steeper) at low E_{rot} and hotter (shallower) at high E_{rot}. The deviation from linearity and therefore the size of the error bars in figure 2(b), becomes marked across the *E*/*H* switchover (beginning at ∼120 W) as might be expected considering the potential greater thermal inhomogeneity. Nevertheless, and again comparing with a simple *in-extremis* model (arms 300 K, 123 mTorr and chamber 600 K, 100 mTorr), we note that in this case the values of T_{rot} appear to be a much better approximation to the actual line-of-sight average gas temperature (in the simple model, accounting for gas dilation, this is ∼360 K).

3.2. Measurements on O_2 (X, $v = 1$)

Figure 3(a) shows several CRD spectra of the $^rQ_{11}(16)$, $^rR_{12}(17)$ and $^rQ_{11}(22)$ rotational transitions within the (1,1) vibrational band of the *b*–X system as a function of plasma power at 100 mTorr (13.332 Pa). Spectra were also obtained for the $^rR_{12}(7)$ transition. Transitions from higher and lower *J* states were too weak to be observed at 0 W hence the more limited range of rotational states probed compared to the $v = 0$ level. Line-of-sight averaged number densities for each rotational state are shown in figure 3(b). The behaviour for $v = 1$ is very different to that seen for $v = 0$, with all rotational states showing a consistent increase in number density with increasing power. This observation arises from the fact that, apart from the small density of $v = 1$ molecules present at 294 K (even when there is no plasma), $v = 1$ is produced mainly by the plasma discharge and hence as power increases so does the density of $v = 1$ regardless of rotational state. The apparent translational temperatures, T_{trans}, calculated from the Doppler widths of these transitions are shown in figure 4(a). All rotational lines show similar increases from near ambient temperatures at low powers up to ca. 600 K at 300 W. These temperatures are elevated compared to those measured previously for $O(^3P)$ (450 K at 300 W) and are in fact closer to those measured by optical emission. This indicates that additional $v = 1$ molecules that are produced by the plasma (i.e. the population over and above the ambient thermal $v = 1$ population and which dominates the absorption measurement at higher

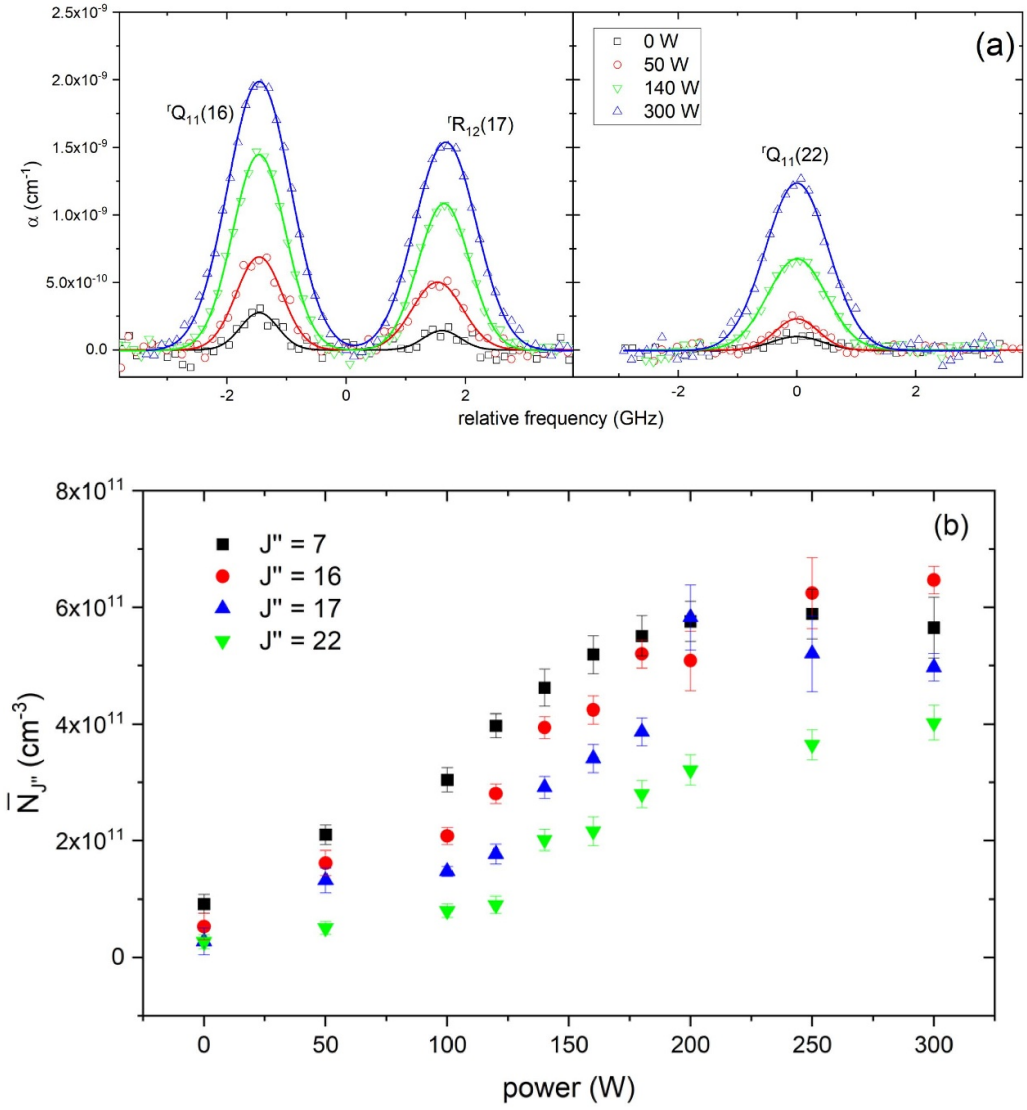

Figure 3. Example CRD spectra of several rotational lines in the (1, 1) band of the O_2 *b*–X system. Panels (a) show lines originating from $J = 16$, 17 and $J = 22$ for different plasma powers. (b) Variation in line-of-sight averaged rotational-state-specific number densities with plasma power. In notable contrast to the vibrational ground state, the $v = 1$ densities all increase with increasing power. Spectra in (a) are centred on 389 835.033 GHz (13 003.497 cm^{-1}) and 389 996.831 GHz (13 008.894 cm^{-1}), in the left and right panes, respectively.

plasma powers) are largely confined to the hot central region of the plasma and that as they leave this region they are quickly quenched (the dominant loss process being *V*–*T* energy transfer with O(^{3}P) [28]), such that there is only ever a small ambient thermal population in the arms. To a good approximation, therefore, plasma produced $v = 1$ molecules fill, at most, 35 cm of the CRDS cavity (i.e. the full chamber diameter with no penetration into the arms).

As before, Boltzmann plots at each plasma power were constructed to calculate both rotational temperatures, $T_{\rm rot}$ and total line-of-sight averaged $v = 1$ number densities, $N_{v=1}$. In this case there is little evidence of non-linearity, indicating that it is the contrast between the *J*-state-populations in the arms and the chamber that mainly leads to this observation for O_2(X, $v = 0$), which is also exacerbated by probing a wider range of *J*-states for the $v = 0$ state. Rotational temperatures are shown in red in figure 4(b) along with the emission derived temperatures for comparison. The temperatures are similar and increase with power almost identically. The discrepancy in the two temperatures is likely to be a result of the different spatial selections inherent in the two techniques, where it is potentially more difficult to exclude imaging optical emission from hotter areas of the plasma, and perhaps also, but to a much lesser extent the influence of $v = 1$ molecules that are present in the arms at all plasma powers (albeit in small numbers).

Figure 5(a) shows how $N_{v=1}$ increases with power. The line-of-sight averaged number density $N_{v=1}$ is the weighted mean of the average density in the arms, $N_{v=1,a}$, and the average density in the chamber, $N_{v=1,ch}$, where the weightings are the lengths of the two regions, $L_a = 42$ cm and $L_{ch} = 35$ cm respectively, i.e. $N_{v=1}\, l = N_{v=1,a}\, L_a + N_{v=1,ch}\, L_{ch}$.

The $v = 0$ data indicate that, if the chamber is held at 100 mTorr, the arms have line-of-sight average pressure of 123 mTorr. At 0 W the temperature is spatially uniform and

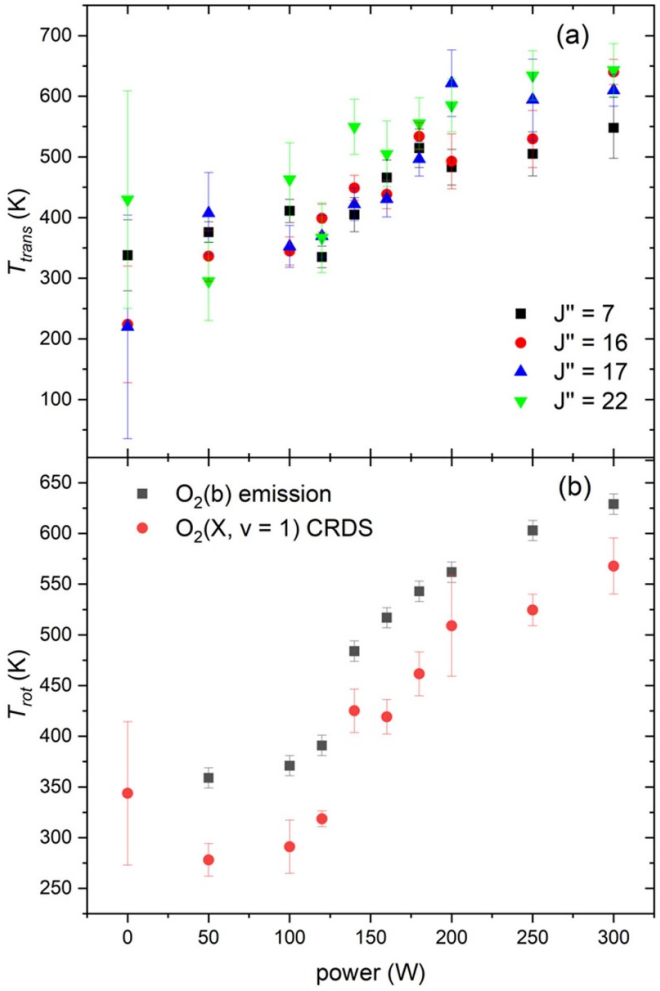

Figure 4. (a) Apparent line-of-sight average translational temperature for the various rotational states of O_2(X, $v = 1$). All rotational states show higher temperatures than were observed for O(^{3}P) and display a significant increase in temperature with power which is broadly in line with the increase observed by emission measurements on the oxygen A-band. This indicates that O_2(X, $v = 1$) and O_2(b) molecules probably have similar spatial distributions and that both are largely absent from the cool baffle arms leading to elevated average temperatures in comparison to O(^{3}P) and O_2(a). We note that the measured absorption coefficients at 0 W are extremely low ($<2.5 \times 10^{-10}$ cm^{-1}) and this precludes an accurate determination of T_{trans} under this condition. (b) Rotational temperatures derived from Boltzmann plots and from the emission data [17] for comparison.

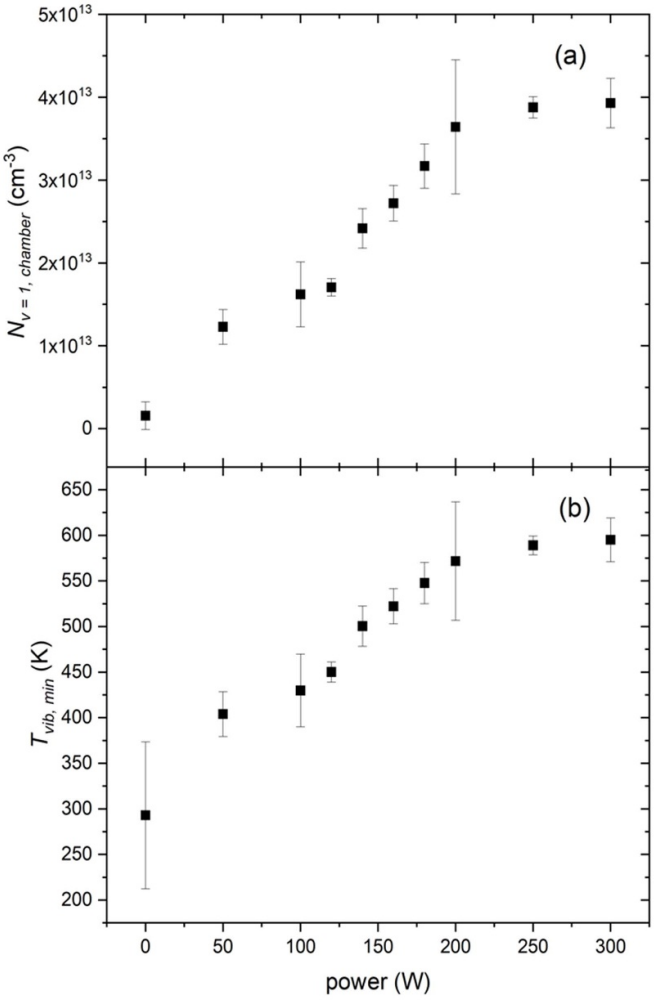

Figure 5. (a) Estimated number density of O_2(X, $v = 1$) assuming that O_2(X, $v = 1$) produced by the plasma is evenly distributed across the entire 35 cm chamber diameter and that the chamber arms contain the same amount of O_2(X, $v = 1$) as when the plasma is off. (b) Vibrational temperatures in the chamber calculated on the basis of the data in (a) and O_2(X, $v = 0$) taken from volume averaged modelling. The values in (a) and (b) should be considered as lower bounds on their respective values because in all likelihood O_2(X, $v = 1$) does not evenly fill the chamber but is in fact found in higher densities near the (translationally and rotationally hotter) chamber centre.

it can be deduced that $N_{v\,=\,1,\,a} = 1.23 N_{v\,=\,1,\,ch}$ under these conditions, i.e. $N_{v\,=\,1,\,a} = 1.93 \times 10^{12}$ cm^{-3}. By assuming that this value of $N_{v\,=\,1,\,a}$ is the same for all plasma conditions the effects of the arms can be subtracted from the data in figure 3(b) and the density of $v = 1$ across the 35 cm of the chamber, $N_{v\,=\,1,\,ch}$, as a function of plasma power can be estimated. This is the data shown in figure 5(a). It should be noted that this method inherently assumes that the vibrational heating by the plasma is uniform across the 35 cm diameter of the plasma chamber. If, as is suspected from the elevated $v = 1$ translational temperatures, the production of $v = 1$ is confined to a slightly smaller (and hotter) region in the centre of the chamber then the density of $v = 1$ molecules in this region would be higher. The values in figure 5(a) are thus lower bounds on the $v = 1$ density in the centre of the chamber.

The $v = 1$ densities can be combined with the densities of O_2(X) from volume averaged modelling [17] to estimate the vibrational temperature in the plasma as a function of power (noting that because $N_{v\,=\,0} \gg N_{v\,=\,1}$ it can reasonably be approximated that the density of O_2(X) predicted by the model is equal to $N_{v\,=\,0}$). Vibrational temperatures, T_{vib}, calculated based on these assumptions are shown in figure 5(b). It should be noted that, because the $v = 1$ densities are lower bounds, so too are the vibrational temperatures. At 300 W a T_{vib} of 600 K is found as a lower bound. Previously emission measurements resulted in an upper bound of 900 K[18] and thus

it can be said with confidence that the line-of-sight average vibrational temperature across the 35 cm of the plasma chamber is 750 ± 150 K. It should also be noted that there is significant evidence that the population of vibrational states in oxygen plasmas are not well described by a Boltzmann distribution with a single vibrational temperature. In particular, Annusova *et al* [28] suggest that high vibrational levels can have populations much higher than would be expected based on the vibrational temperature apparent amongst the lower vibrational levels, thus the calculated vibrational temperatures are only applicable in defining the populations of lower vibrational levels, i.e. $v \leqslant \approx 2$. The vibrational distribution function of Annusova *et al* indicates a vibrational temperature, defined by the ratio of $v = 1$ and $v = 0$ populations, of ≈1000 K for an 80 mTorr, 500 W plasma and, bearing in mind the slightly different plasma conditions, this is in reasonable agreement with the value of 750 ± 150 K found here (100 mTorr, 300 W).

4. Discussion and modelling

In order to further interpret the O_2 (X, $v = 0$) data presented above some level of spatially resolved modelling is required. In this section we present a simple one-dimensional model and show that it can provide some quantitatively useful results. The basis of this model is to approximate the variation in pressure, translational/rotational temperature, and mole fractions as a function of position along the propagation axis of the CRDS cavity, which defines the z-axis. These inputs then allow expected line-of-sight averaged temperatures and number densities of the various species (including different rotational states of molecules) to be predicted and compared with experiment. The pertinent equations are now described and are applied for plasma operating conditions of 100 mTorr, 300 W.

Feedstock gas entering the plasma chamber passes along the baffle arms and this flow is necessarily associated with a pressure gradient. The pressure change along a length of tube with a gas flow can be estimated using the Poiseuille equation for an ideal gas [29]:

$$p(L) = \sqrt{p_0^2 + \frac{16\mu Q_0 p_0}{\pi R^4} L}, \tag{3}$$

where $p(L)$ is the pressure at position L along the tube, p_0 is the pressure in the chamber, μ is the dynamic viscosity of the gas, Q_0 is the volumetric flow at $L = 0$ (i.e. the chamber/arm interface) and R is the baffle arm radius. Defining the origin as the centre of the chamber such that the cavity mirrors are located at $z = \pm 0.385$ m, it is then possible to define an approximate piecewise function $p(z)$ that describes the line-of-sight pressure variation:

$$\begin{array}{ll} \sqrt{p_0^2 - AQ_0p_0(z+0.175)} & -0.385 \leqslant z \leqslant -0.175 \\ p_0 & -0.175 \leqslant z \leqslant 0.175 \\ \sqrt{p_0^2 + AQ_0p_0(z-0.175)} & 0.175 \leqslant z \leqslant 0.385 \end{array}, \tag{4}$$

where $A = (16\mu/\pi R^4)$ and $p_0 = 100$ mTorr (13.332 Pa). For oxygen at 300 K, $\mu = 2 \times 10^{-5}$ kg s^{-1} m^{-1} [30] and for a flow of 5 sccm along each arm flowing into a chamber held at 100 mTorr, $Q_0 = 6.934 \times 10^{-4}$ m^3 s^{-1}; for the baffle arms in this work, we have chosen $R = 5.7 \times 10^{-3}$ m to match the observation that under these conditions the average arm pressure is 123 mTorr (164 Pa). This seems reasonable as while most of the arm is dominated by a 10 mm internal diameter tube, there are some regions where it is slightly larger (e.g. close to the mirrors and the chamber walls). The pressure variation along the CRDS cavity predicted by equation (4) is shown in figure 6 (top pane).

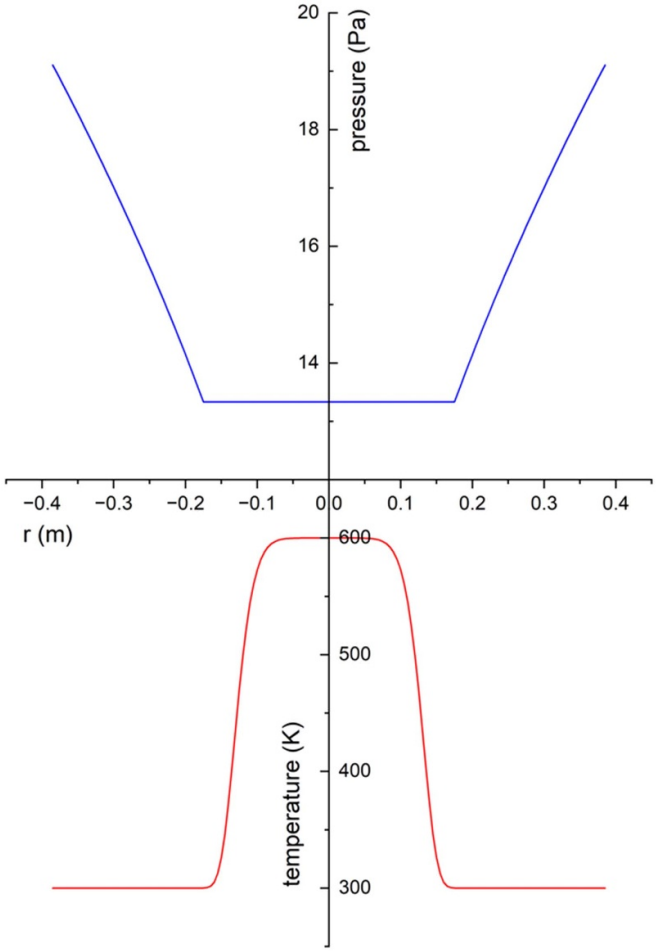

Figure 6. Variation of total pressure along the CRDS cavity (top), pressure in the centre is fixed at 100 mTorr (13.332 Pa) whilst pressure in the baffle arms increases according to the Poiseuille equation. Bottom—an estimate of the spatial variation of the gas rotational and translational temperature in the plasma. The profile is plotted according to equation (5) with parameters chosen as detailed in the text to give a physically reasonable approximation.

For the purposes of this 1-d model the gas temperature within the chamber is approximated by a flat-topped Gaussian function (also known as a super-Gaussian [31]) of the form:

$$T(z) = T_0 + \Delta T \exp\left(-\left(\frac{z^2}{b}\right)^a\right), \tag{5}$$

where T_0 is the gas temperature in the baffle arms (taken as 300 K), ΔT is the difference in gas temperature between the arms and the centre of the chamber (taken as 300 K, in

other words assuming the central chamber is at 600 K based roughly on optical emission data [17]) and a and b are parameters that define how steeply the temperature drops from its maximum value and the extent of the hottest region respectively. The temperature profile, used in calculating the expected line-of-sight integrated densities and temperatures for a 300 W plasma, uses values of $a = 4$ and $b = 0.018$ and is shown in figure 6 (lower pane). This profile is physically reasonable because its hottest region is approximately the same diameter as the driven coil and the temperature drops to 300 K at ± 0.175 m, i.e. where the plasma meets the cooled chamber wall.

The spatial variation in mole fractions, $x(z)$, of the various species in the plasma is also required. While the experimental data presented here are concerned with O_2(X), we focus our modelling [17] on three species of interest—these are $O(^3P)$, $O_2(a)$ and O_2(X, $v = 0$) ($v = 1$ molecules show evidence of being confined to the hottest region of the plasma and are thus less interesting from the point of view of spatially resolved modelling). Mole fractions for the plasma borne species, x_i, are calculated from the densities returned in our volume averaged model [17] while mole fractions of these species in the baffle arms are found using the exponential decay lengths determined from experimentally measured wall loss coefficients; these decay lengths are 0.5 cm for $O(^3P)$ and 5 cm for $O_2(a)$, respectively. Thus, the mole fraction of atomic oxygen, x_O, is approximated as:

$$x_O(z) = \begin{array}{ll} 0.12763\exp\left(\frac{z+0.175}{0.005}\right) & -0.385 \leqslant z \leqslant -0.175 \\ 0.12763 & -0.175 \leqslant z \leqslant 0.175 \\ 0.12763\exp\left(\frac{0.175-z}{0.005}\right) & 0.175 \leqslant z \leqslant 0.385 \end{array}. \tag{6}$$

For $O_2(a)$, the mole fraction, x_a, has the same functional form as in equation (6) but with an amplitude of 0.056 79 reflecting its lower abundance and with a longer exponential decay length, reflecting the lower wall loss coefficient for $O_2(a)$ on the steel baffle arm walls. Finally, the mole fraction of O_2(X, $v = 0$), x_{X0}, is approximated as $x_{X0} = (1 - x_O - x_a)$.

The line-of-sight averaged translational temperature for species i, $T_{trans,i}$, is calculated according to:

$$T_{trans.i} = \frac{\int T(z) N_i(z)\,dz}{\int N_i(z)\,dz} = \frac{\int p(z) x_i(z)\,dz}{\int \left(\frac{p(z)x_i(z)}{T(z)}\right) dz}, \tag{7}$$

and for each molecular species the line-of-sight averaged temperature expected for a particular rotational state can be calculated by noting that the mole fraction of the Jth rotational state of species i, x_J, is given by:

$$x_J(z) = x_i(z)\frac{(2J+1)\exp\left(-\frac{E_{rot}}{k_B T(z)}\right)}{q_{rot}}, \tag{8}$$

where q_{rot} is the rotational partition function. For a diatomic molecule, $q_{rot} \propto T(z)$ and by replacing $x_i(z)$ in equation (7) with x_J given by equation (8), one finds the line-of-sight average temperature for a particular rotational state:

$$T_{trans} = \frac{\int p(z) x_i(z) \frac{\exp\left(-\frac{E_{rot}}{k_B T(z)}\right)}{T(z)} dz}{\int p(z) x_i(z) \frac{\exp\left(-\frac{E_{rot}}{k_B T(z)}\right)}{T(z)^2} dz}. \tag{9}$$

The model can therefore be used to predict line-of-sight averaged temperatures for each rotational state (and for $O(^3P)$) and these can be compared directly to the measurements for each transition. For $O(^3P)$ the model predicts a line- of-sight averaged temperature of 476 K which compares very favourably with our previously reported temperatures in the H-mode $\approx 450 \pm 20$ K. The modelled and measured values for the rotational states of O_2(X, $v = 0$) and $O_2(a, v = 0)$ are shown in figures 7(a) and (b) respectively, where we obtain rotational-state-specific density and apparent T_{trans} information for $O_2(a, v = 0)$, ($J = 4$, 6,10,12) from data presented in Rogers *et al* [19]. The modelled translational temperatures for O_2(X) show a much stronger rotational state dependence than those for $O_2(a)$ and this simply reflects the different distributions of the various rotational states along the line-of-sight of the cavity.

Given the simplicity of the model and the many assumptions it makes, the agreement with the O_2 (X, $v = 0$) data is good, with the model always within ≈ 40 K and much better than that for higher rotational states. The model also reproduces very well the variation of apparent T_{trans} with rotational state energy and this strongly supports the explanation given previously that the Doppler line widths vary due to the different spatial distributions of the various rotational states. The agreement for $O_2(a)$ is poorer but we note that the data for this species are significantly less certain given the markedly smaller absorption coefficients measured.

Finally, the line-of-sight averaged number density of a given species i are calculated using:

$$N_i = \frac{1}{L}\int N_i(z)\,dz = \frac{1}{k_B L}\int \left(\frac{p(z)x_i(z)}{T(z)}\right) dz. \tag{10}$$

For individual rotational states of molecules equation (8) can be substituted into equation (10) to give:

$$N_J = \frac{(2J+1)}{k_B L}\int p(z) x_i(z) \frac{\exp\left(-\frac{E_{rot}}{k_B T(z)}\right)}{q_{rot}(z) T(z)} dz, \tag{11}$$

and numerical solutions can be obtained using $q_{rot}(z) = 0.7215\, T(z)$ for O_2(X, $v = 0$) and $q_{rot}(z) = 0.481\, T(z)$ for $O_2(a, v = 0)$; these relationships are obtained from linear fits to q_{rot} values calculated by PGOPHER and are very close to the rigid rotor limits for both molecules when spin multiplicities and Λ-doubling are accounted for. For $O(^3P)$ the distributions described above predict a line-of-sight averaged number density of 1.21×10^{14} cm^{-3} in very good agreement with the experimental value of 1.25×10^{14} cm^{-3}. Figures 7(c) and (d) show the modelled and measured line-of-sight average densities in each rotational state of O_2(X, $v = 0$) and $O_2(a, v = 0)$ that was measured. The agreement for ground state molecules is again remarkably good whilst the agreement

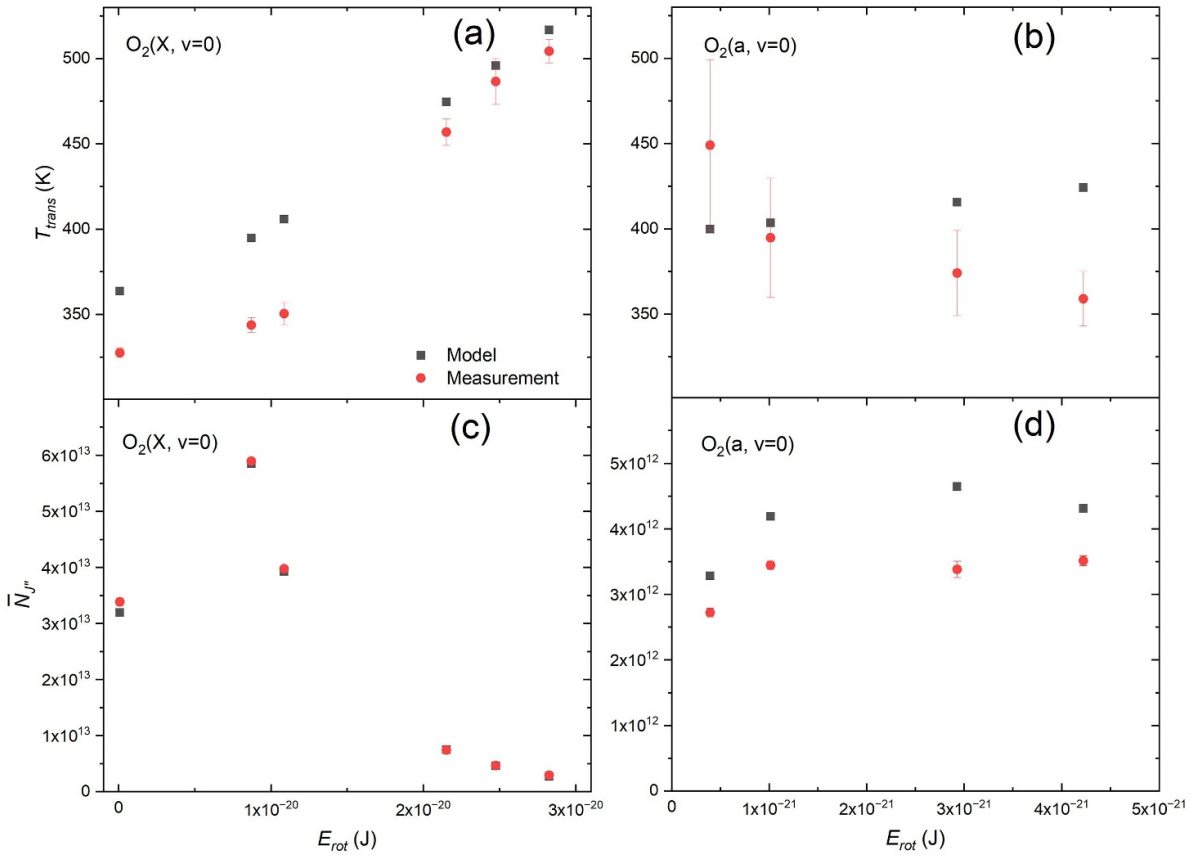

Figure 7. Modelled and measured line-of-sight average temperatures as a function of rotational energy for (a) O_2(X, v = 0) and (b) O_2(a, v = 0). Modelled and measured line-of-sight average number densities as a function of rotational energy for (c) O_2(X, v = 0) and (d) O_2(a, v = 0). O_2(a) line-of-sight measurements are derived from data in Rogers *et al* [19].

for the first metastable is reasonable and the modelled values demonstrate the correct trend with rotational energy.

5. Conclusions

Previous spectroscopic studies on important low energy atomic and molecular states produced in low pressure oxygen plasma show that these different species tend to exhibit different translational and rotational temperatures, with those that are longest lived e.g. $O_2(a)$, apparently possessing lower temperatures than those with shorter lifetimes, e.g. $O_2(b)$. This observation led to the hypothesis that the plasma has significant thermal inhomogeneity, with long lived species having sufficient lifetimes to thermally equilibrate with the cool chamber walls and also to penetrate a significant distance into the cold baffle arms.

In order to test this hypothesis CRDS measurements have been performed on the $v = 0$ and $v = 1$ states of O_2(X), the principal component in the plasma. The $v = 0$ state, which fills the majority of the arms, showed cold (<350 K) line-of-sight averaged translational temperatures unless very highly excited rotational states were probed. Such rotational states ($J = 28, 30, 31$) only exist with significant population when the temperature is significantly above ambient and are hence largely confined to the plasma region and are not found in the baffle arms. O_2 (X, $v = 1$) meanwhile is translationally hot (≈550 K) across all rotational states as a result of it being produced only in the hot plasma and then lost rapidly if it leaves this region. This hypothesis is supported by a simple model of plasma inhomogeneity whereby the pressure, temperature and mole fractions of the various species across the chamber (and arms) are approximated with rational profiles and the corresponding line-of-sight averaged densities and temperatures calculated. This basic model is reasonably successful at reproducing the observations for O_2 (a, $v = 0$) and O(^{3}P). Further detailed insights into spatial inhomogeneity can be gained through effective modelling in order to determine temperature profiles, i.e. utilising physical models that include plasma heating mechanisms and thermal diffusion. These are currently being undertaken and in combination with experimental results could provide insight into thermal accommodation coefficients relevant for this chamber (see for example Gibson *et al* [32]).

In summary, the 1 d model of the plasma described here is, given its simplicity, remarkably successful at reproducing the observed behaviour of several species within the plasma. This illustrates the extent of the thermal inhomogeneity in the H-mode and demonstrates that this inhomogeneity plays a significant role in determining the line-of-sight average densities and apparent temperatures, not just of different species but also of different rotational states of the same species. Moreover, the

fact that resolving several rotational transitions allows spatial variations within the plasma to be inferred from line-of-sight average measurements, is a powerful result that could be of great utility in future work.

Data availability statement

All data that support the findings of this study are included within the article (and any supplementary files).

Acknowledgments

The authors would like to acknowledge the UK Engineering and Physical Sciences Research Council (EPSRC) for support provided within the standard research scheme (Grant No. EP/P026621/1) and Lam Research Corporation (US) for a gift award. SDAR would like to thank the Clarendon fund for the award of a graduate scholarship.

ORCID iDs

Samuel D A Rogers https://orcid.org/0000-0002-5276-0920
Amelia Bond https://orcid.org/0000-0002-9539-6698
Robert Peverall https://orcid.org/0000-0003-2326-2495
Gus Hancock https://orcid.org/0000-0003-1166-4104
Grant A D Ritchie https://orcid.org/0000-0003-1663-7770

References

[1] Gudmundsson J T, Kouznetsov I G, Patel K K and Lieberman M A 2001 *J. Phys. D: Appl. Phys.* **34** 1100–9
[2] Franklin R N 2001 *J. Phys. D: Appl. Phys.* **34** 1834–9
[3] Kiehlbauch M W and Graves D B 2003 *J. Vac. Sci. Technol.* A **21** 660–70
[4] Yang W and Wolden C A 2006 *Thin Solid Films* **515** 1708–13
[5] Langowski B A and Uhrich K E 2005 *Langmuir* **21** 6366–72
[6] Chan C M, Ko T M and Hiraoka H 1996 *Surf. Sci. Rep.* **24** 1–54
[7] Milliron D J, Hill I G, Shen C, Kahn A and Schwartz J 2000 *J. Appl. Phys.* **87** 572–6
[8] Krastev V, Reid I, Galassi C, Hughes G and McGlynn E 2005 *J. Mater. Sci., Mater. Electron.* **16** 541–7
[9] Singh M K, Ogino A and Nagatsu M 2009 *New J. Phys.* **11** 115027
[10] Gudmundsson J T, Marakhtanov A M, Patel K K, Gopinath V P and Lieberman M A 2000 *J. Phys. D: Appl. Phys.* **33** 1323–31
[11] Corr C S, Gomez S and Graham W G 2012 *Plasma Sources Sci. Technol.* **21** 055024
[12] Gudmundsson J T, Kimura T and Lieberman M A 1999 *Plasma Sources Sci. Technol.* **8** 22–30
[13] Meichsner J and Wegner T 2018 *Eur. Phys. J.* D **72** 85
[14] Hancock G, Peverall R, Ritchie G A and Thornton L J 2007 *J. Phys. D: Appl. Phys.* **40** 4515–8
[15] Booth J P, Guaitella O, Chatterjee A, Drag C, Guerra V, Lopaev D, Zyryanov S, Rakhimova T, Voloshin D and Mankelevich Y 2019 *Plasma Sources Sci. Technol.* **28** 055005
[16] Booth J P *et al* 2020 *Plasma Sources Sci. Technol.* **29** 115009
[17] Rogers S D A, Bond A, Rhodes B J, Peverall R, Hancock G and Ritchie G A D 2022 *Plasma Sources Sci. Technol.* **31** 115006
[18] Peverall R, Rogers S D A and Ritchie G A D 2020 *Plasma Sources Sci. Technol.* **29** 045004
[19] Rogers S D A, Bond A, Peverall R, Hancock G, Western C M and Ritchie G A D 2021 *Plasma Sources Sci. Technol.* **30** 09LT02
[20] Wegner T, Küllig C and Meichsner J 2017 *Plasma Sources Sci. Technol.* **26** 025006
[21] Fuller N C M, Malyshev M V, Donnelly V M and Herman T P 2000 *Plasma Sources Sci. Technol.* **9** 116
[22] Bakowski B, Hancock G, Peverall R, Ritchie G A and Thornton L J 2004 *J. Phys. D: Appl. Phys.* **37** 2064–72
[23] Romanini D, Kachanov A A and Stoeckel F 1997 *Chem. Phys. Lett.* **270** 538
[24] Western C M 2017 *J. Quant. Spectrosc. Radiat. Transfer* **186** 221–42
[25] Yu S, Drouin B J and Miller C E 2014 *J. Chem. Phys.* **141** 174302
[26] Drouin B J *et al* 2017 *J. Quant. Spectrosc. Radiat. Transfer* **186** 118
[27] Gordon I E *et al* 2022 *J. Quant. Spectrosc. Radiat. Transfer* **277** 107949
[28] Annusova A, Marinov D, Booth J P, Sirse N, Silva M L D, Lopez B and Guerra V 2018 *Plasma Sources Sci. Technol.* **27** 045006
[29] Landau L D and Lifshitz E M 1987 *Fluid Mechanics* 2nd edn (Permagon Press)
[30] Lemmon E W and Jacobsen R T 2004 *Int. J. Thermophys.* **25** 21–69
[31] Parent A, Morin M and Lavigne P 1992 *Opt. Quantum Electron.* **24** 1071–9
[32] Gibson A R, Foucher M, Marinov D, Chabert P, Gans T, Kushner M J and Booth J P 2017 *Plasma Phys. Controlled Fusion* **59** 024004